Sensory experience controls dendritic structure and behavior by distinct pathways involving degenerins

Sharon Inberg, Yael Iosilevskii and Benjamin Podbilewicz*

Department of Biology, Technion-Israel Institute of Technology, 3200003 Haifa, Israel

* Benjamin Podbilewicz
Department of Biology, Emerson Building, Room 4-31
Technion-Israel Institute of Technology, 3200003 Haifa, Israel
Tel +972 4 8293454
Email: podbilew@technion.ac.il

Author Contributions: SI and BP conceived and designed the experiments. SI performed the experiments. YI conceived, designed and performed the gait experiments. SI, YI and BP analyzed the data and wrote the paper.

Competing Interest Statement: None

Classification: Biological Sciences. Neuroscience

Keywords: Dendritic plasticity, *Caenorhabditis elegans,* Epithelial sodium channels(degenerins)

This PDF file includes:

Main Text
Figures 1 to 6

Abstract

Dendrites are crucial for receiving information into neurons. Sensory experience affects the structure of these tree-like neurites, which, it is assumed, modifies neuronal function, yet the evidence is scarce, and the mechanisms are unknown. To study whether sensory experience affects dendritic morphology, we use the *Caenorhabditis elegans'* arborized nociceptor PVD neurons, under natural mechanical stimulation induced by physical contacts between individuals. We found that mechanosensory signals induced by conspecifics affect the dendritic structure of the PVD. Moreover, developmentally isolated animals show a decrease in their ability to respond to harsh touch. The structural and behavioral plasticity following sensory deprivation are functionally independent of each other and are mediated by an array of evolutionarily conserved mechanosensory amiloride-sensitive epithelial sodium channels (degenerins). Our genetic results, supported by optogenetic, behavioral, and pharmacological evidence, suggest an activity-dependent homeostatic mechanism for dendritic structural plasticity, that in parallel controls escape response to noxious mechanosensory stimuli.

Significance Statement

Little is known about how neuronal activity and sensory experience influence the structure and function of dendritic trees. Furthermore, how dendritic structures affect neuronal functions remains obscure despite their fundamental functions in neuronal sensory and synaptic activities in health and diseases. Here we show that complex dendritic trees of the nociceptive and proprioceptive PVD neuron in *C. elegans* display a dynamic nature where they undergo pronounced dendritic modifications during adulthood. These modifications are determined by the received sensory signals generated by conspecific worms in the plate. We revealed functions for degenerins/Epithelial sodium channels in this phenomenon, using genetic and optogenetic approaches. We found that degenerins serve to translate environmental mechanical signals into structural and functional modifications in the PVD.

Main Text

Introduction

The general structure of the nervous system has been known for over a century. Groundbreaking studies on synaptic plasticity and its underlying mechanisms have shown that before birth and in adult animals, neuronal activity is needed for synaptic remodeling (1-5). In contrast, the molecular mechanisms responsible for structural remodeling of dendritic trees, as a result of different sensory inputs (experience), especially during adulthood, are less understood (6-8).

Mechanistic understanding of experience-dependent structural plasticity is primarily focused on activity sensation by calcium channels and N-methyl-D-aspartate (NMDA) receptors. These are known to induce downstream signaling cascades affecting, among others, the Rho family of small GTPases, calcium metabolism and microtubule stability (9-12). Several neurological conditions including autism, Down syndrome, fragile X syndrome, and schizophrenia are characterized by abnormal dendritic spine structures (13-16). Uncovering the molecular basis of dendritic tree instability during development and adulthood, may shed light on neurological disease mechanisms and elucidate their behavioral phenotypes.

The dendrite morphology of the *Caenorhabditis elegans'* PVD bilateral neurons is composed of repetitive, stereotypical and spatially organised structural units that resemble candelabra (Fig. 1A), making it a useful platform to study dendritic morphogenesis (17). While some of the genetically-programmed molecular mechanisms responsible for the morphogenesis and regeneration of PVD's dendritic trees are known (17-25), the influence of nurture, e.g. sensory experience, on its structure and function during development and in adulthood remain unexplored. The PVD mediates three sensory modalities (reviewed in (26)): response to harsh mechanical stimuli (nociception) (27), response to low temperatures (27) and proprioception (28, 29). While the PVD response to low temperatures is mediated by transient receptor potential (TRP) channels (27), nociception and proprioception are mediated by degenerins/epithelial Na^+ channels (DEG/ENaCs) expressed in the PVD (27, 30), which form homo- and hetero-trimers and are involved in force sensing. In mammals, some DEG/ENaCs such as ASIC1a participate in synaptic plasticity and cognitive functions such as learning and memory (31-38). As sensory and social isolation affect the behavior and fitness of diverse animals (39-42), including primates (43), studying adult nematode somatosensory neurons can reveal possibly-conserved mechanisms of dendritic plasticity, which are induced by sensory stimuli.

In gentle touch circuits, which are distinct from nociception (17, 44, 45), Rose et al (46) found that deprivation of mechanosensory stimulation generated by colliding conspecifics in the growing plate, resulted in modified glutamatergic signalling and reduced response to tap stimulation. Here, we adapted this mechanosensory stimulation paradigm (46), where the crowded worms are thought to represent the natural 'default' enriched mechanosensory state, to look into nociceptive circuits and

identify the mechanism that couples mechanosensory experience to structural and functional dendritic plasticity. We focused on how mechanosensory experience, perceived through DEG/ENaCs, affects structural plasticity of the PVD dendritic trees in adult *C. elegans*, and whether this entails behavioral consequences. We find that mechanosensory experience not only alters the PVD's dendritic structure in the adults, but also affects associated behavioral outputs. However, and in contrast to the prevalent hypothesis, these structural and behavioral properties are not correlated.

Results

Sensory isolation induces behavioral plasticity

Rose et al., (46) has shown that isolation of wildtype (WT) *C. elegans* causes a decreased response to gentle touch circuits when comparing to worms raised in a crowded setting. We utilized a similar paradigm to study nociception, a behavior associated with PVD neuron activation (17, 47), using a behavioral assay that registers escape following prodding with a platinum wire (harsh touch assay; Fig. 1A) (17, 44, 45). To study whether mechanosensory deprivation affects the nociceptive functions of the PVD, we isolated embryos into single plates where they grew 72 h to adulthood and compared their behavioral response to harsh touch against same-aged adults that were grown on crowded plates (Fig. 1B). We found that ~40% of isolated WT animals responded to harsh touch, compared with ~80% of animals grown in crowded plates (Fig. 1C). To test whether gentle touch neurons are involved in this behavioral difference, we studied *mec-4(e1611)* mutants, in which gentle touch neurons are degraded (44, 48-51), and obtained similar results (Fig. 1C). Given that *mec-4(e1611)* exhibits the same experience-dependent behavioral plasticity as WT, we conclude that this phenomenon is independent from the *mec-4* gentle-touch neurons. As a negative control, we used *mec-3(e1338)* mutants, that are harsh-touch-insensitive (47) and found no responses for both groups (Fig. 1C). Thus, isolation reduces the response to noxious stimuli, in a process that is independent of gentle touch circuits.

To determine whether the effect of isolation on nociception is related to the mechanosensory deficit itself (like friction (52) and collisions (27), in contrast to chemosensory stimuli), we used the *mec-4* strain to compare responses of isolated worms to responses of isolated worms grown in the presence of glass beads (resembling a method used by (53)). Worms grown in isolation with beads had a similar response compared to animals grown in crowded plates (Fig. S1A). While the beads are sufficient to increase isolated animals' responses, they do not fully recapitulate the crowded state (Fig. S1A). To study whether the effect was chemosensory-mediated, we tested plates pre-stimulated with pheromones as well as *osm-6* mutants (defective in olfactory sensory cilia (54)). We found that isolation induced a reduction in the response to harsh touch, regardless of plate 'odour' (Fig. 1D) or chemosensory function (Fig. S1B). We note that the chemosensory defective *osm-6* mutants also have a defective ciliated mechanosensory PDE neuron (54) (which mediates posterior harsh touch responses (44)). These results suggest that adult worms display a behavioral plasticity

131 in PVD-related harsh touch circuits, which is dependent on mechanosensory
132 experience, and is independent of the PDE neuron, olfactory and gentle touch neurons.

133 To provide further evidence to the involvement of PVD-related neuronal circuitry,
134 we have examined a second behavioral output, associated with the PVD's modality of
135 proprioception (position in space) (28, 29). By recording and analyzing adult worms'
136 movement patterns, we found that isolated animals showed a significant increase in
137 crawling amplitude and wavelength compared with crowded counterparts (Fig. S2A and
138 B; Movies S1 and S2). To determine whether gentle touch neurons are involved in this
139 behavioral difference, we tested *mec-4(e1611)* mutants and obtained similar results
140 (Fig. S2A and B). In contrast, *mec-3(e1338)* mutants, which are harsh-touch-
141 insensitive, showed no significant difference in crawling amplitude and a decrease in
142 wavelength and speed in isolated worms compared to crowded conditions (Fig. S2).
143 Thus, isolation affects the gait by increasing the amplitude and wavelength, in a process
144 that is independent of gentle touch circuits.

145 **MEC-10 and other mechanosensory channels mediate isolation-induced**
146 **behavioral plasticity before adulthood**

147 To study the genetic mechanisms behind the nociceptive response plasticity, we
148 performed a candidate gene screen for degenerins (DEG/ENaC) and transient receptor
149 potential (TRP) channels that are expressed in the PVD, where degenerins mediate
150 mechanosensation and proprioception, while TRPs sense low temperatures. In all these
151 signal transduction pathways some of the outcomes are behavioral responses (27, 55).
152 We found that the WT-like isolation-induced reduction in harsh touch response was also
153 present in *degt-1* DEG/ENaC and *gtl-1* TRP channel mutants, suggesting that these
154 channels are not directly involved in behavioral plasticity following isolation (Fig. 1E). In
155 contrast, for *del-1*, *asic-1* and *mec-10* DEG/ENaC mutants the difference between
156 isolated and crowded conditions was undetectable, indicating that they are required for
157 such behavioral plasticity. Interestingly, while the harsh touch response of *asic-1*
158 mutants was consistently high, and similar to crowded WT worms, the response for
159 *mec-10* mutants was consistently low, similar to isolated WT animals, regardless of
160 sensory experience (Fig. 1E). To test whether the response to harsh touch is dependent
161 on DEG/ENaC activity, we used the DEG/ENaC blocker amiloride (32, 56) on WT
162 worms that were grown in crowded plates. We found that the response to harsh touch
163 was not affected by continuous growth in the presence of amiloride (Fig. S1C). This
164 result possibly supports the idea that different amiloride-sensitive epithelial sodium
165 channels may have positive and negative effects on the response to harsh touch, which
166 are masked by global inhibition (Fig. 1E). This is further evident by the plasticity
167 consequences of some double and triple DEG/ENaC mutant combinations, which are
168 difficult to align into an epistatic genetic model (Fig. S9).

169 The DEG/ENaC MEC-10 is expressed in the PVD and responds to
170 mechanosensory signals (27) including shear forces (52, 57). Since crowded *mec-10*
171 mutants seem isolated-like in their behavioral response (Fig. 1E), we asked how *mec-*
172 *10* mediates the behavioral plasticity in crowded conditions. To test whether the activity

173 of MEC-10 is required autonomously in the PVD, we expressed MEC-10 under a PVD-
174 specific promoter in a *mec-10* mutant background (17, 58) 22, 49, 58). We found that
175 expression of MEC-10 in the PVD rescues the low response to harsh touch in crowded
176 *mec-10* mutants, indicating that it acts cell autonomously to modulate behavioral
177 plasticity (Fig. 1F).

178 To determine whether isolation affects the response to harsh touch during
179 development or in adults, we isolated crowded-raised young adults for 24 h and found
180 no difference in their response to harsh touch (Fig. 1G). Thus, isolation-induced
181 reduction in mechanosensation is determined before young adults, is PVD cell-
182 autonomous, and *mec-10*-dependent. To determine whether the proprioceptive
183 differences noted following isolation also depend on *mec-10*, we repeated the
184 movement analysis in *mec-10* mutants. We found that in *mec-10* mutants the amplitude
185 and wavelength were similar in isolated and crowded conditions (Fig. S2; Movies S3
186 and S4), suggesting that MEC-10 influences both nociceptive and proprioceptive
187 plasticity following isolation.

188 **Experience affects PVD morphology via *mec-10* in adulthood**

189 Sensory experience (such as stimuli deprivation) is known to drive synaptic plasticity in
190 the nervous system (3, 4, 59). However, little is known about the effects of
191 mechanosensory deprivation on the architecture of sensory neurons. To study whether
192 reduced mechanosensory experience can alter the dendritic structure of the PVD we
193 followed the isolated growth paradigm (Fig. 1B) and examined two morphological
194 features of the PVD (Fig. 2A): The fraction of ectopic (excessive, disordered) branches
195 out of non-ectopic branches (those that form the 'ideal' candelabrum), and the
196 percentage of straight 4th order (quaternary) branches, which form the terminal
197 processes of the candelabrum.

198 When quantifying the branching pattern of the PVD in adulthood, WT (or WT-like
199 *him*-5 background) animals which were isolated as embryos showed an increase in
200 ectopic branching compared with crowded age-matched worms (Fig. 2B) and the
201 quaternary branches assumed a more rippled shape (fewer straight 4ry branches, Fig.
202 2C), regardless of the neuron marker utilized (see Fig. S3).

203 To determine whether chemical stimulation plays a role in the observed
204 morphological plasticity, animals were isolated onto pheromone-conditioned plates (60).
205 Similarly to the response to harsh touch (Fig. 1D), chemical stimulation of the plates did
206 not rescue the isolation-induced increase in the fraction of ectopic branching or the
207 decrease in percentage of straight quaternary branches (Fig. S4). Additionally, we
208 looked at *mec-4* gentle-touch-insensitive mutants (46, 51) and found that isolation
209 caused a similar change to PVD structure as in the WT (Fig. S5, compare with Fig. 2B
210 and 2C). In summary, these results suggest that mechanosensory experience controls
211 morphological plasticity of PVD dendritic trees independently of *mec-4* and chemical
212 stimulation.

We next sought to determine whether DEG/ENaCs mediate these experience-driven morphological alterations, by examining PVD morphology in crowded and isolated *mec-10* mutants. We found that crowded *mec-10* animals were different from WT crowded worms, and appear more isolated-like in terms of morphological features (more ectopic branches and fewer straight quaternary branches, compared to crowded *him-5* control animals; Fig. 2B and 2C). These results suggest that PVD dendritic morphology is affected by sensory experience in a *mec-10*-dependent pathway. Importantly, these results confirm a role for the mechanosensory channel MEC-10, but not other degenerins (such as ASIC-1), in the plasticity of both the dendritic structure and the nociceptive function of the PVD in the crowded background.

To study whether *mec-10* acts cell autonomously to mediate morphological plasticity, we again utilized PVD-specific MEC-10 expression in a *mec-10* mutant background and found it reduced the fraction of ectopic branches and increased the percentage of straight quaternary branches, compared to age-matched crowded *mec-10* animals without the rescue array (Fig. 2D-I). Thus, MEC-10 acts in the PVD to mediate morphological plasticity.

Having identified an isolation-induced morphological plasticity in adults (observed at 72 h from embryo), we next sought to establish the temporal dependence of the effect by comparing animals after only 48 h, as young adults (see Fig. S6A). Isolated worms showed a small but significant difference for the percentage of straight quaternary branches, but not in ectopic branching (Fig. S6B-E) when compared with age-matched crowded worms, suggesting that isolation induces some morphological alterations during morphogenesis while some relate to adult-stage maintenance of the neuron. We then isolated animals grown for 48 h in crowded conditions, and found that isolation of young crowded adults for 24 h induced changes in both measured parameters (Fig. S6F-I), recapitulating isolation of embryos (Fig. 2B-C). Thus, isolation of adults for 24 h is sufficient to affect PVD dendritic tree architecture, in contrast to the developmentally-established behavioral response (Fig. 1G).

To further determine whether the morphological effect on PVD structure is solely mediated by mechanical cues, we used glass beads under isolated conditions. We found that while the presence of glass beads did not reduce the fraction of ectopic branching, it significantly increased the number of straight quaternary branches (compared with isolated animals without beads, Fig. 2J-K). Thus, the mechanosensory stimuli of inert beads can partially rescue isolation-induced morphological changes to the PVD.

Isolation triggers dynamic plasticity of the dendritic tree

To pinpoint the precise time interval required to mediate dendritic arborization changes in adulthood, we examined the effect of varying isolation times on the PVD morphology of crowded-raised young adults. We found that isolation of adults for 2 h had no significant consequence on the structure of the PVD, while isolation of adults for 5 h or

253 more significantly increased the proportion of ectopic branches and reduced the
254 percentage of quaternary straight branches compared to crowded worms (Fig. 3A-B).

255 To further study plasticity at the individual level, we compared the dendritic tree
256 of individual worms grown under crowded conditions before and after 4 h isolation. This
257 revealed isolation induced more events of ectopic branch growth and fewer events of
258 branch retraction (Fig. 3C). Furthermore, this period was sufficient to induce an increase
259 in ectopic branching and a decrease in percentage of straight quaternary branches
260 (Figs. 3D, 3E, and S7). Thus, 4 h of isolation are sufficient to induce changes in the
261 architecture of the adult PVD.

262 Since the geometry of quaternary branches shows rapid response to the amount
263 of mechanosensory stimulation (Fig. 3A-E), we next asked how dynamic is this
264 experience-dependent morphological change. We performed a 3 h time lapse imaging
265 in crowded and isolated animals anesthetized with 1% tricaine (Movies S5 and S6). We
266 found that while the number of straight quaternary branches in the isolated worms
267 remained low and stable (~8%), for the crowded animals, we observed a gradual
268 reduction in straight quaternary branches, starting after ~2 h of isolation of individual
269 worms on the slide (Fig. 3F,G).

270 In summary, isolation-induced morphological plasticity is apparent within 2-3 h
271 from the switch from crowded conditions to growth in the absence of mechanical stimuli.
272 This dynamic process involves simultaneous increase in ectopic branching and
273 decrease in straight terminal branches.

274 **Activity affects morphology**

275 It has been shown that activity and sodium influx via the DEG/ENaC UNC-8 promotes
276 synapse elimination in *C. elegans* (61). To test how global inhibition of DEG/ENaCs
277 affects the morphology of the PVD neuron, we evaluated crowded worms that were
278 grown on plates with amiloride compared to control worms. We found that blocking
279 DEG/ENaCs by amiloride increased the fraction of ectopic branching and decreased the
280 percentage of straight quaternary branches (Fig. S8A-D). Thus, unlike harsh touch
281 response, which is independent of sensory-level global inhibition (Fig. S1C), global
282 inhibition at the sensory level alters dendritic morphology. These results suggest that
283 activity via degenerins modulates the structure of the PVD.

284 To test whether manipulations of other neuromodulators can affect the branching
285 dynamics of the PVD, we utilized two anesthetics: tetramisole, which activates the
286 nematode nicotinic acetylcholine receptors inducing muscle contraction (62) and
287 tricaine, which modulates neuronal activity by blocking sodium channels (63) and
288 analyzed their effects during 2-3 h of time lapse movies of crowded and isolated
289 animals. We first tested the commonly used mixture of 0.1% tricaine and 0.01%
290 tetramisole (the racemic mixture of the enantiomer levamisole) (21) and found that it
291 induces more growth than retraction of ectopic branches in crowded animals (Fig. S8E-
292 G). In contrast, 1% tricaine alone has the opposite effect- more retractions of ectopic
293 branches (Fig. S8H-I; Movies S5 and S6). In addition, 1% tricaine induces more growth

294 for isolated compared to crowded worms, indicating that there are activity-dependent
295 intrinsic factors that are different for the two experience states. These results suggest
296 that modulating neuronal activity triggers structural modifications in the PVD, indicating
297 a possible structural sensitivity to the amount of neuronal activity. In summary, we found
298 that mechanosensory experience, DEG/ENaC protein presence and activity, and
299 pharmacological targeting of activity dynamically affect the structure of the PVD.

300 **PVD structure and function are independent**

301 After establishing that mechanosensory experience induces both a behavioral and a
302 structural plasticity of the PVD, we asked whether there is a causal link between the
303 morphology of the dendritic tree of the PVD and its function as a nociceptor (64). We
304 followed the isolation protocol described in Fig. 1B for seven combinations of
305 DEG/ENaC mutants and analyzed their response to harsh touch (Fig. S9) and their
306 PVD structure (Fig. S10). In order to compare the morphological properties of the
307 different DEG/ENaC genotypes under different sensory experience (crowded, isolated;
308 Fig. S10), we used discriminant analysis. This provides a supervised classification
309 method to combine all the analyzed morphological phenotypes, including loss of self-
310 avoidance between adjacent candelabra (Fig S11), into a certain value characterizing
311 the PVD morphological state (Fig. 4A). We then superimposed the behavioral results of
312 the DEG/ENaC mutants' response to harsh touch (Fig. S9) on the morphological
313 clustering, as a binary-like property (<45% responding for isolated WT versus >65% for
314 crowded WT, as shown in Fig. S9*)*. We found no correlation between the morphology of
315 the PVD and the response to harsh touch when testing the different combinations of
316 genotypes and treatments. For example, isolated *mec-10;degt-1* double mutants show
317 crowded-like morphology with isolated-like behavioral response (Fig. 4A and Fig. S9,
318 S10). These findings suggest that while degenerins are required for isolation-induced
319 plasticity of both traits, response to harsh touch is independent of the structural
320 alteration of the PVD.

321 An additional line of evidence supporting the independence of the behavioral and
322 morphological phenotypes was demonstrated by isolation of young adult worms for 24 h
323 (Fig. 3). This isolation affects the structure of the PVD (Fig. S6) but has no effect on the
324 response to harsh touch (Fig. 1G). Amiloride also has no effect on harsh touch
325 response (Fig. S1C) but does alter dendritic morphology (Fig S8 A-D). Finally, to directly
326 demonstrate that these two features are independent, we assayed harsh touch
327 responses of isolated animals and then analyzed each individual animal for its PVD
328 morphology. We then compared the dendritic morphology of responding and non-
329 responding worms, and found that the morphological parameters were similar (Fig. 4B-
330 E). Thus, analysis at the level of individual worms failed to demonstrate a correlation
331 between the morphology and the response to harsh touch. In summary, the
332 morphological and behavioral phenotypes were independently affected by sensory
333 experience via degenerins. We cannot exclude the possibility that other functions of the
334 PVD, like the response to low temperatures (27) and proprioception (28) are more tightly
335 associated to the structure of the PVD, nor that the morphological changes induced by
336 isolation are too minor to constitute a difference in neuronal function.

In addition to the isolation-induced changes in the number of ectopic branches and the percentage of straight quaternary branches, we found that worms raised in isolation are also more likely to lose the self-avoidance between two adjacent menorahs (candelabra). This effect is also *mec-10*-dependent, but appears to act cell non-autonomously. In addition, it is chemosensory and amiloride independent (Fig. S11).

MEC-10 and DEGT-1 localization is experience-dependent

Differential localization of degenerins can affect both the behavioral response to harsh touch and the structural properties of the neuron. When considering the effect of isolation, we hypothesized that changes in the localization patterns of DEG/ENaC can account for plasticity at both the behavioral (Fig. 1) and the structural level (Figs. 2, 3). Since MEC-10 and DEGT-1 tend to co-localize within the PVD (27), we analyzed the interaction between these two proteins, under different mechanosensory experiences. We found that MEC-10 localization in the plasma membrane, in intracellular vesicular compartments of the axon and in the quaternary branches was reduced after isolation (Fig. 5A-D, Movies S7 and S8). In contrast to MEC-10 (Figs. 5A-D), DEGT-1 localization is reduced only in the cell body following isolation (Fig. 5E-H). Furthermore, *degt-1* mutants reduced the overall amount of MEC-10, and more importantly, abrogated the isolation-induced reduction in MEC-10 localization at the quaternary branches and the axon (Fig. 5A-D). In the reciprocal experiment, DEGT-1 localization was affected in *mec-10* mutants, as isolated worms exhibit increased localization to the cell body compared with WT isolated worms (Fig. 5E-H). Thus, mechanosensory experience also induces plasticity in the localization pattern of MEC-10 and DEGT-1. We propose this differential localization may be part of the mechanism that independently and locally modulates dendritic and axonal properties, to affect both the structure and the function of the PVD, respectively.

Optogenetic stimulation suggests behavioral plasticity is post-sensory

We have shown that sensory deprivation (isolation) affects the localization of two different mechanoreceptors, the degenerins MEC-10 and DEGT-1 in the dendrites, axon and soma of the PVD. It is conceivable that the differential localization of degenerins in different domains of the PVD may affect the morphology and function of the PVD. Thus, we decided to stimulate the PVD independently of the endogenous mechanoreceptors and study whether the escape behavior following harsh touch is similar in isolated and crowded animals. We hypothesized that if we circumvent the normal degenerin-mediated mechano-stimulation, exciting the PVD downstream to sensory activity, the animals grown in isolation will respond to the same degree as if they were in crowded conditions and independently of the dendritic tree morphology. Optogenetic stimulation is an elegant way to bypass the sensory perception mediated by receptors and transduced by diverse signal transduction pathways (30). Thus, to investigate whether the isolation-induced decreased response to harsh touch is a PVD-dependent function, we used optogenetic stimulation with Channelrhodopsin (ChR2) expressed in the PVD (30). We found that isolation significantly reduced the percentage of worms responding to optogenetic stimulation of the PVD (Fig. 5I), indicating that the

379 plasticity in the response is acting downstream to PVD activation, mechanosensory
380 channels and signal transduction pathways. This activation is sensitive to isolation
381 probably because it is acting pre- or post-synaptically. To determine whether
382 optogenetic stimulation of isolated animals can reverse the morphological changes
383 induced by the absence of mechanical stimuli in PVD, we used optogenetic stimulation
384 of the PVD and found no significant difference between isolated and isolated-
385 optogenetically-stimulated animals in terms of any measured PVD structural
386 characteristic (data not shown). Thus, optogenetic stimulation on isolated animals is not
387 sufficient to convert their dendritic trees to crowded-like. In addition, isolated animals
388 respond to optogenetic stimulation in a reduced way suggesting that the escape is not
389 dependent on the dendritic trees but on pre- or post-synaptic pathways. In summary,
390 genetic, pharmacological and optogenetic evidence show that dendritic structural
391 plasticity is an autonomous activity-dependent homeostatic mechanism. The
392 mechanosensory dendritic tree morphology is independent from pre- or post-synaptic
393 degenerin-mediated processes that affect behavioral escape in response to harsh
394 touch.

395 **Discussion**

396 From the evolutionary point of view, dendritic trees and their structural complexity
397 remain mysterious objects, despite many efforts to understand the contribution of
398 arborization complexity to dendritic physiology and function (65).

399 Previous research has demonstrated both cell autonomous (17, 18, 66) and cell
400 non-autonomous (19, 20) mechanisms that regulate the PVD's dendritic morphogenesis
401 during development. Some studies have also focused on regeneration and aging effects
402 on the tree structure of the PVD, revealing plasticity in the adult stage (21, 22), similar to
403 what has been shown for *Drosophila* sensory neurons (67). We found, by using mutants
404 for degenerins, chemosensory stimulation controls, pharmacology, optogenetics and
405 glass beads, that the dendritic structure of the PVD and the behavioral response to
406 harsh touch are activity- and mechanosensory-dependent, but appear to be
407 chemosensory-independent. It is still conceivable that chemosensation can affect
408 nociception and proprioception, in some sort of a cross modal plasticity mechanism, but
409 at the moment we do not have evidence for this scenario in the PVD, where we show
410 that mechanosensory channels (DEG/ENaCs) affect the architecture of the PVD.

411 Our results suggest that 'nurture', manifested as mechanosensory experience,
412 activates mechanotransduction signaling, via DEG/ENaCs amiloride-sensitive activity,
413 to stabilize the homeostatic structure of the dendritic tree in adults. The sensory
414 experience induced when one body side of the worm is in contact with the agar plate is
415 not sufficient for this purpose (data not shown); however, other worms on the plate, or
416 the presence of glass beads, elicit significant structural alterations. Moreover, the cell
417 autonomous activity of MEC-10 in the PVD was found to be both necessary and
418 sufficient to preserve the crowded-experience phenotype in terms of the simplified
419 structure of the PVD. While there are other multiple plausible explanations, our failure in
420 remodeling the isolated-state arbor by repeated optogenetic activation of the PVD may
421 provide further evidence for the necessity of degenerins in this structural plasticity, since

422 neuron activation by ChR2 bypasses the activation of mechanically-gated degenerin
423 channels. Figure 6 depicts our working model, where the amount of mechanosensory
424 stimulation, in crowded or isolated conditions, affects the expression and localization of
425 MEC-10 and DEGT-1 in different compartments of the PVD. Localization of MEC-10,
426 probably by forming higher-order complexes with other DEG/ENaCs, can affect the
427 structure of the PVD at the level of the dendritic tree. The morphological and behavioral
428 phenotypes shown here were rescued by a PVD-specific expression of MEC-10,
429 supporting such a cell autonomous mechanism. The experience-induced structural
430 plasticity seems homeostatic at the individual branch dynamics level in the adult. In
431 contrast, we show that the behavioral response to harsh touch is modulated by
432 mechanosensory experience during development and by the presence of degenerins,
433 and perhaps involves other neurons downstream. Based on optogenetic stimulation, we
434 presume that the behavioral plasticity is a pre- and/or post-synaptic property, mediated
435 by DEG/ENaC (36) and related to neurotransmission modulation, independently of the
436 structure of the PVD dendritic tree. These structural and behavioral plasticity are
437 separated in time (adulthood vs. development) and space (dendrite vs. axon; Fig. 6).
438 We found no correlation or causation between the structure and the nociceptive function
439 of the PVD. It is possible that such a link exists, but our physiological and behavioral
440 outputs are not sensitive enough to detect it.

441 Isolation induces changes to crawling gait by increasing crawling amplitude and
442 wavelength. Such changes may be related to the proprioceptive role of the PVD, and
443 are in partial agreement with the effects of PVD ablation on crawling gait (28). This
444 experience-mediated movement alteration persists in a *mec-4(e1611)* background, but
445 is absent in *mec-10* mutants (Fig. S2), leading us to propose this is an independent,
446 behavioural, *mec-10*-mediated plasticity.

447 Tao et al., (29) supports the role of MEC-10 in PVD-mediated proprioception,
448 however has some discrepancies with our results with regard to harsh touch response,
449 which may be related to the different methodologies used, as well as to the animals' age
450 and mechanosensory experience.

451 Somatosensory activation in vertebrates plays a prominent role in shaping the
452 structural and functional properties of dendritic spines, mainly studied in the central
453 nervous system (68-71). In contrast to mammalian cortical neurons, much less is known
454 about sensory neurons' degree of plasticity and the molecular mechanisms utilized
455 during adulthood. Here we suggest that degenerins mediate mechanosensation-
456 induced dendritic growth in sensory dendrites. The dendritic plasticity we described
457 bears resemblance to the activity-dependent effect of glutamatergic signaling and
458 NMDA receptors. Activity via NMDA affects dendritic spines as an upstream mechanism
459 of cell signaling, resulting in structural modifications (72-75). It is possible that
460 degenerins mediate mechanosensory signaling sensation, by activating cationic
461 gradients (76), leading to activation of downstream intracellular signaling pathways (9-
462 12), which in turn stabilize local, actin-mediated (3, 77, 78) structural plasticity in the
463 PVD dendritic branches. In parallel, DEG/ENaCs may also modulate pre- and post-

464 synaptic homeostatic signaling in the harsh touch circuit, as has been shown in
465 neuromuscular junctions (79).

466 In summary, we propose that the combinatorial actions of DEG/ENaCs have
467 mechano-signaling functions mediating plasticity in sensory dendritic trees, and provide
468 mechanistic insights into dendritic structural responses to sensory experience in
469 adulthood and the behavioral consequences of such adaptations during development.
470

471 **Materials and Methods**

472 **Strains**
473 Nematode strains were maintained according to standard protocols (80). The list of the
474 strains is presented in Supplementary Table 1. Strains of the DEG/ENaCs family
475 obtained from the CGC (JPS282: *asic-1*(*ok415*) I; ZB2551: *mec-10*(*tm1552*) X; VC2633:
476 *degt-1*(*ok3307*) V) were crossed with BP709: *hmnIs133[ser-2Prom3::kaede]*. The
477 validation of F2 homozygotes for the DEG/ENaCs deletions (including single, double
478 and triple mutants) was performed by PCR amplification of the genomic area containing
479 the deleted region.

480 **Primers for Multiplex PCR**
481 The list of the primers used is presented in Supplementary Table 2.

482 **Spinning disk confocal microscopy**
483 Prior to imaging, the worms were mounted on a 10% agar pad placed on a microscope
484 glass slide, in 1µl polystyrene beads (100 nm diameter; *Polysciences*, Inc.) for their
485 mechanical restraint, and sealed with a coverslip for complete physical immobilization
486 (81). The PVD neuron was visualized using a Yokagawa CSU-X1 spinning disk, Nikon
487 eclipse Ti inverted microscope and iXon3 camera (ANDOR). Images were captured with
488 MetaMorph, version 7.8.1.0. For each worm, a sequential z-series image stack (step
489 size of 0.35 µm) was obtained with an oil Plan Fluor 40X (NA 1.3) lens around the PVD
490 cell body, encompassing approximately 50-100 µm segments both anteriorly and
491 posteriorly.

492 **Data analysis**
493 The analysis of the PVD structure was performed for the area surrounding the cell body.
494 All images were analysed with ImageJ, version 1.48 (NIH), in TIFF format, by producing
495 a maximal intensity z-series projection and converting it to negative form (invert lookup
496 table) for improved visibility. Ectopic branching was defined as described previously
497 (65). Briefly, non-ectopic branches form the 'ideal' WT candelabrum of the late L4 stage,
498 whereas excess branches, which create non-quaternary terminal ends, are considered
499 ectopic, as illustrated with dashed lines for ectopic branching in Fig. 2A. The total
500 number of ectopic and non-ectopic branches was quantified for each image, and
501 presented as a fraction (ectopic/non-ectopic branches).
502 The geometry of each quaternary branch ("candle") was defined in the following
503 manner: Straight geometry- all the pixels that constitute the branch are positioned on a
504 straight line generated with ImageJ. The width of the line (1 pixel) was constant for the

entire sets of experiments. The number of straight quaternary branches were divided by the total quaternary branches in the image for each worm and presented as a percentage. The analysis was done only for worms which did not move through the Z series. Moving worms were excluded from the experiment. Self-avoidance defects- the number of events where two adjacent candelabra overlapped (no gap formation), was divided by the total number of gaps between the candelabra within the frame (Fig. 2A). The self-avoidance values are presented as percentage.

Behavioral procedures

Harsh touch assay

After 72 h, adult worms (both isolated and those from the crowded plate as described below) were transferred using an eyelash each to a new agar plate, freshly seeded with 150 µl OP50 (about 16 h after seeding). This step is required to avoid a thick edge of the bacterial lawn, which might interfere with harsh touch response measurement. After ~45 minutes in the plate, the worms were prodded with a platinum wire posterior to the vulva, above the interface between worm's body and the agar plate (47), every 10 seconds, and the number of responses to harsh touch was counted. More than one response constitutes a responsive animal. The non-responding worms were defined if two prodding events were observed sequentially without response. The percentage of responding worms was calculated for each genotype and treatment. The experimenter was blind to both the genotype and the treatment- crowded or isolated.

Isolation of embryos

The worm isolation procedure was based on previous work (46) with a few modifications, as indicated. Isolated animals were grown on 6 cm agar plate with 150 µl of OP50 *E. coli*, while crowded plate worms were grown on 600-700 µl OP50 to prevent starvation. The embryos and adult worms were isolated with platinum wire. The plates were sealed with one layer of Parafilm M and placed into a plastic box, at 20 ºC, for the entire experiment.

Three experimental groups were used for the 72 h (96 h of experiment was performed only for *mec-4* worms, since they were L4- very young adults at 72 h) isolation experiment: **(1)** Single isolated embryos **(2)** Crowded worms - the progeny of 30 young, non-starved, adults (approximately, 7,000-9,000 worms in different developmental stages, without approaching starvation) **(3)** Crowded adult worms that were isolated for a certain amount of time as adults.

After 48/72/96 h (according to the experiment), age-matched worms from each group were transferred to 10% agar pad slides for imaging, as described above (46).

Isolation of adults for 2, 5, 15 or 24 hours

Crowded plates were prepared as described above, with progeny from 30 adult hermaphrodites. Animals were separated into individual plates for the desired time window before 72 h have passed (*i.e.* after ~70 h for 2 h isolation, ~67 h for 5 h isolation etc.). Worms were isolated using an eyelash into new plates containing 150 µl of OP50. At 72 h, the PVD of isolated animals was imaged and compared with age-matched animals which remained in the crowded plate of origin (see Fig. 1B).

547 **Optogenetics stimulation for harsh touch**
548 Crowded and isolated worms (ZX819: *lite-1(ce314) X;*
549 *xIs12[pF49H12.4::ChR2::mCherry; pF49H12.4::GFP*]) were grown on OP50 with 100
550 µM All Trans Retinal (ATR, Sigma R2500), in order to obtain functional
551 Channelrhodopsin (30) (as a control we tested the response of worms that were grown
552 on ethanol alone, no response was detected for these worms). After 72 h the worms
553 were singly mounted with eyelash on a chunk (1cm X 1cm) of agar that was mounted
554 on a microscope glass slide. The agar contained fresh but dry OP50, with 100 µM ATR.
555 About 30 minutes following the transfer the worms were tested for the response to light.
556 Worms were stimulated at 488 nm wavelength, with laser intensity of 40% and exposure
557 time of 100 ms, with 10X Plan Fluor (NA 0.3) for ~1 second and the forward
558 acceleration response was measured. The microscope system is as described above.
559 The experimenter determined the presence or the absence of forward acceleration in
560 response to light activation.

561 **Optogenetics stimulation of isolated worms**
562 Isolated eggs were grown as described at the 'Isolation of embryos' section.
563 Isolated worms (ZX819: *lite-1(ce314) X; xIs12[pF49H12.4::ChR2::mCherry;*
564 *pF49H12.4::GFP*]) were grown on 150 µM OP50 with 100 µM ATR (30) or 0.3% ethanol
565 as control. After 72 h both the crowded and isolated worms were singly mounted with
566 eyelash onto a cube (with surface area of about approx.1cm^2, depth of 0.5 cm) of agar
567 layered with fresh, fully dried, OP50 with 100 µM ATR or 0.3% ethanol as a control
568 group. The worms were stimulated with 488 nm wavelength, with laser intensity of 40%
569 and exposure time of 100 ms, with 10X Plan Fluor (NA 0.3) for ~60 seconds, every 5
570 min during 4 h. Stimulation and recording was performed with the microscope system
571 described above.
572 As a control, before each experiment, crowded ZX819 worms were tested for forward
573 acceleration as a positive control to the functionality of the ChR2. After the end of 4 h
574 stimulation, the worms were mounted for imaging of the PVD at 40X as described under
575 "Spinning disk confocal microscopy" section.

576 **Isolation with chemical stimulation**
577 The *glp-4(bn2)* mutants which are sterile at 25 °C were used (~40 worms for each
578 plate), in order to prepare conditioned/chemically stimulated plates (60) prior to growing
579 isolated animals. The *glp-4* mutants were transferred at early larval stage (L1, L2) to a
580 new agar plate for 96 h at 25 °C. After the removal of the *glp-4* mutants, the embryo
581 isolation procedure was used, as described before at 20 °C.

582 **Isolation with glass beads**
583 Single embryos were isolated to agar plates with 150 µl OP50 and 2.5 g of glass beads
584 (1 mm diameter) were placed on the OP50 lawn in the middle of the plate. The worms
585 were isolated for 72 h and tested for response to harsh touch as described above.

586 **Pharmacology**
587 Amiloride hydrochloride hydrate (Sigma, #A7410) 1 M stock solution in DMSO was
588 stored at -20°C. A final concentration of 3 mM amiloride in 0.03 % DMSO was prepared

589 in OP50 bacteria (LB medium) and seeded on NGM plates. 650 µl of the OP50 mixture
590 was seeded on each plate. As a control, 0.03 % DMSO was added to OP50 bacteria.
591 For each plate (control 0.03% DMSO or 3 mM amiloride) 30 non-starved adult worms
592 were added. After 72 h at 20 °C the progeny of the 30 adults were tested as young
593 adults for their PVD morphology and their response to posterior harsh touch, as
594 described in the previous sections.

595 **Anesthetics and long-term imaging**
596 In addition to immobilization of worms with 100 nm polystyrene beads as described in
597 the ”Spinning disk confocal microscopy” section above, two additional methods for long
598 term imaging and pharmacological effects assays were used: 1% tricaine (Sigma,
599 A5040) in M9 buffer or a mixture of 0.01% tetramisole (Sigma, T-1512) and 0.1%
600 tricaine in M9 buffer were utilized.
601 Worms were exposed to the anesthetics (in a glass well) for ~20 min until paralyzed,
602 then transferred to 3% agar pads with 1 µl of the anesthetics. Sequential z-axis image
603 series (0.6 µm step-size) were taken, as described above, every 5 min for 2-3 h.

604 **Imaging individual worms- crowded to isolated**
605 Worms were grown at crowded conditions, as described above. At ~24 h of adulthood,
606 individual worms were placed in a 1% tricaine solution in M9 buffer for 10 min until
607 paralyzed and transferred to 3% agar slides with 1 µl 1% tricaine. Following a short
608 PVD imaging session, the worms were recovered from the slide with M9 and isolated to
609 a new plate for 4 h. Each 4 h-isolated animal was anesthetized once again with 1%
610 tricaine for 10 min prior to PVD imaging.

611 **Analysis of DEG/ENaCs localization in the PVD**
612 Two DEG/ENaCs protein constructs, pF49H12.4::MEC-10::mCherry and
613 pF49H12.4::DEGT-1::mCherry (plasmids kindly provided by W. Schafer’s lab, (27))
614 were analysed for their localization in the PVD, by comparing worms expressing the co-
615 injection marker *punc-122*::GFP raised in crowded or isolated conditions, in a similar
616 behavioral assay as described in Fig. 1B. A z-series (step size of 0.35 µm,
617 immobilization performed with polystyrene beads, as described in the microscopy
618 section) of the area around the cell body of the PVD was obtained with a 60X
619 Apochromat (NA 1.4) lens. The images (after maximal intensity projection of the Z-
620 series) were encoded so the analysis was performed in a blind manner. The presence
621 or absence of fluorescent signal was examined in three compartments: The cell body,
622 the quaternary branches and the axon of the PVD.

623 **Rescue strains**
624 Worms from BP1022 (*mec-10(tm1552)* X; *hmnIs133[ser-2Prom3::Kaede]*; *him-5(e1490)*
625 V) were injected into the gonad with a rescuing plasmid for *mec-10*, with a PVD specific
626 promoter (pWRS825: *ser-2Prom3::mec-10* genomic) kindly provided by W. Schafer’s
627 lab (27). The injection mix contained *myo-2p::GFP* (20 ng/µl) as a co-transformation
628 marker and pWRS825 (80 ng/µl). For both behavioral and structural characterization,
629 the *him-5;mec-10* strains, with and without rescuing plasmid, shared the same crowded
630 plate and were differentiated by the presence or absence of the co-injection marker.

631 **Crawling gait analysis**
632 Crowded and isolated animals were grown for 72 h to young adults as described above
633 in 'Isolation of embryos'. Four to six hours prior to the experiment, NGM plates were
634 seeded with 100-120 µl OP50 and dried to a transparent matte finish (seeking to avoid
635 a darkened circle edge when recording). Six to eight worms at a time were transferred
636 using an eyelash to the test plates, left to recover for five minutes, and videotaped for
637 10-12 minutes on an illuminator table (MBF Bioscience, Williston, VT, USA) at 7.5
638 frames/second with a resolution of 2592×1944 using an overhanging fixed lens (Nikon
639 AF Micro-Nikkor 60 mm f/2.8D) focused at 10 µm/pixel.

640 From each video, recorded in monochrome AVI (Audio Video Interleaved) format, a
641 section of three minutes was subsequently analyzed using the WormLab software (MBF
642 Bioscience) to recover average values of worm length, crawling speed, wavelength and
643 amplitude. The three-minute section was taken from the beginning of the video, unless
644 worms were lost, absent, or stuck, at which case a later section was analyzed.
645 Providing for segments of poor tracing, which were manually removed, each worm was
646 tracked for 100-180 seconds in total. Excepting *mec-3(e1338)*, animals which left the
647 OP50 patch for longer than 30 s or whose analyzed average speed was lower than 50
648 µm/s were excluded from the analysis, as these behaviors are likely to skew the results.
649 *mec-3* animals, which were inherently markedly slower, were kept in the analysis even if
650 their speed was lower than 50 µm/s.

651 **Statistics and data plotting**
652 At least two independent experiments constitute the data set described in each figure.
653 For the morphological characterization of the PVD the results are expressed as means
654 (blue circle) ± standard error of the mean (s.e.m.). In the boxplot (first, third quartiles)
655 the upper whisker extends from the hinge to the highest value that is within 1.5 * IQR
656 (inter-quartile range), the distance between the first and third quartiles. The lower
657 whisker extends from the hinge to the lowest value within 1.5 * IQR of the hinge.
658 The statistical analyses were performed with SPSS software (IBM, version 20) and "R
659 package". Two-tailed tests were performed for the entire data sets.
660 Since for many experiments the distribution of the data was not normal, nonparametric
661 tests were used: Mann-Whitney test for comparison between two independent groups.
662 Kruskal-Wallis test was used for multiple comparisons for more than two groups.
663 For proportions (percentage worms) ± standard error of proportion was calculated.
664 Fisher's exact test was used for analysis of differences in proportions. To estimate the
665 variability in proportion we calculated the Standard Error of Proportion: $\sqrt{\frac{(1-p)\cdot p}{n}}$
666 The dot plot figures were prepared with "R package", the bar charts with Microsoft Excel
667 software. Final figures were prepared with Adobe Illustrator CS version 11.0.0.

668 **Discriminant analysis**
669 Eight different strains (WT and seven DEG/ENaCs), with two treatments (crowded,
670 isolated worms) for each strain were analyzed for Linear discriminant analysis for
671 morphological characteristics, to evaluate similarity between different strains and
672 treatments. Each worm in the data set was characterized by the three morphological

characteristics (the fraction of ectopic branching, the percentage straight quaternary branches and the percentage of self-avoidance defects). The centroid for morphological characterization was calculated for each condition and represented by a square. Data from independent harsh touch experiments are shown for each group. The analysis was performed using SPSS 20.

Acknowledgments

We thank current and former lab members for their intellectual and technical support. Veronika Kravtsov, Sagi Levy, Anna Meledin, Meital Oren-Suissa, Tom Shemesh, Shay Stern, Yehuda Salzberg and Alon Zaslaver for critically reading and commenting on the manuscript. Ehud Ahissar, Dan Cassel, Michel Labouesse and Kang Shen for fruitful discussions. William Schafer, Max Heiman and Alexander Gottschalk for plasmids and strains. Some strains were provided by the Caenorhabditis Genetics Center (CGC), which is funded by NIH Office of Research Infrastructure Programs (P40 OD010440). This work was supported by grants from the Israel Science Foundation (442/12 and 257/17), Adelis Fund (2023479), and the Ministry of Science and Technology (3-13022).

References

1. L. C. Katz, C. J. Shatz, Synaptic activity and the construction of cortical circuits. *Science* **274**, 1133-1138 (1996).
2. C. S. Goodman, C. J. Shatz, Developmental mechanisms that generate precise patterns of neuronal connectivity. *Cell* **72 Suppl**, 77-98 (1993).
3. Y. Zuo, G. Yang, E. Kwon, W. B. Gan, Long-term sensory deprivation prevents dendritic spine loss in primary somatosensory cortex. *Nature* **436**, 261-265 (2005).
4. K. Fox, R. O. Wong, A comparison of experience-dependent plasticity in the visual and somatosensory systems. *Neuron* **48**, 465-477 (2005).
5. T. Wiesner *et al.*, Activity-Dependent Remodeling of Synaptic Protein Organization Revealed by High Throughput Analysis of STED Nanoscopy Images. *Front Neural Circuits* **14**, 57 (2020).
6. G. Tavosanis, Dendritic structural plasticity. *Dev Neurobiol* **72**, 73-86 (2012).
7. B. Kolb, I. Q. Whishaw, Brain plasticity and behavior. *Annu Rev Psychol* **49**, 43-64 (1998).
8. R. O. Wong, A. Ghosh, Activity-dependent regulation of dendritic growth and patterning. *Nat Rev Neurosci* **3**, 803-812 (2002).
9. W. C. Sin, K. Haas, E. S. Ruthazer, H. T. Cline, Dendrite growth increased by visual activity requires NMDA receptor and Rho GTPases. *Nature* **419**, 475-480 (2002).
10. A. E. Ghiretti *et al.*, Rem2 is an activity-dependent negative regulator of dendritic complexity in vivo. *J Neurosci* **34**, 392-407 (2014).
11. Z. Zhou *et al.*, Brain-specific phosphorylation of MeCP2 regulates activity-dependent Bdnf transcription, dendritic growth, and spine maturation. *Neuron* **52**, 255-269 (2006).
12. A. R. Vaillant *et al.*, Signaling mechanisms underlying reversible, activity-dependent dendrite formation. *Neuron* **34**, 985-998 (2002).
13. Y. N. Jan, L. Y. Jan, Branching out: mechanisms of dendritic arborization. *Nat Rev Neurosci* **11**, 316-328 (2010).

717 14. H. T. Hu, T. N. Huang, Y. P. Hsueh, KLHL17/Actinfilin, a brain-specific gene associated
718 with infantile spasms and autism, regulates dendritic spine enlargement. *J Biomed Sci*
719 **27** (2020).
720 15. J. L. Huebschman, K. S. Corona, Y. Guo, L. N. Smith, The Fragile X Mental Retardation
721 Protein Regulates Striatal Medium Spiny Neuron Synapse Density and Dendritic Spine
722 Morphology. *Front Mol Neurosci* **13** (2020).
723 16. H. Tendilla-Beltran, R. Antonio Vazquez-Roque, A. Judith Vazquez-Hernandez, L.
724 Garces-Ramirez, G. Flores, Exploring the Dendritic Spine Pathology in a Schizophrenia-
725 related Neurodevelopmental Animal Model. *Neuroscience* **396**, 36-45 (2019).
726 17. M. Oren-Suissa, D. H. Hall, M. Treinin, G. Shemer, B. Podbilewicz, The fusogen EFF-1
727 controls sculpting of mechanosensory dendrites. *Science* **328**, 1285-1288 (2010).
728 18. Y. Salzberg, N. J. Ramirez-Suarez, H. E. Bulow, The proprotein convertase KPC-1/furin
729 controls branching and self-avoidance of sensory dendrites in *Caenorhabditis elegans.*
730 *PLoS Genet* **10**, e1004657 (2014).
731 19. Y. Salzberg *et al.*, Skin-derived cues control arborization of sensory dendrites in
732 *Caenorhabditis elegans*. *Cell* **155**, 308-320 (2013).
733 20. X. Dong, O. W. Liu, A. S. Howell, K. Shen, An extracellular adhesion molecule complex
734 patterns dendritic branching and morphogenesis. *Cell* **155**, 296-307 (2013).
735 21. V. Kravtsov, M. Oren-Suissa, B. Podbilewicz, The fusogen AFF-1 can rejuvenate the
736 regenerative potential of adult dendritic trees by self-fusion. *Development* **144**, 2364-
737 2374 (2017).
738 22. M. Oren-Suissa, T. Gattegno, V. Kravtsov, B. Podbilewicz, Extrinsic Repair of Injured
739 Dendrites as a Paradigm for Regeneration by Fusion in *Caenorhabditis elegans*.
740 *Genetics* **206**, 215-230 (2017).
741 23. X. Dong, K. Shen, H. E. Bulow, Intrinsic and extrinsic mechanisms of dendritic
742 morphogenesis. *Annu Rev Physiol* **77**, 271-300 (2015).
743 24. C. J. Smith *et al.*, Time-lapse imaging and cell-specific expression profiling reveal
744 dynamic branching and molecular determinants of a multi-dendritic nociceptor in *C.*
745 *elegans*. *Dev Biol* **345**, 18-33 (2010).
746 25. S. Inberg *et al.*, Lessons from Worm Dendritic Patterning. *Annu Rev Neurosci* **42**, 365-
747 383 (2019).
748 26. M. B. Goodman, P. Sengupta, How *Caenorhabditis elegans* Senses Mechanical Stress,
749 Temperature, and Other Physical Stimuli. *Genetics* **212**, 25-51 (2019).
750 27. M. Chatzigeorgiou *et al.*, Specific roles for DEG/ENaC and TRP channels in touch and
751 thermosensation in *C. elegans* nociceptors. *Nat Neurosci* **13**, 861-868 (2010).
752 28. A. Albeg *et al.*, *C. elegans* multi-dendritic sensory neurons: morphology and function.
753 *Mol Cell Neurosci* **46**, 308-317 (2011).
754 29. L. Tao *et al.*, Parallel Processing of Two Mechanosensory Modalities by a Single Neuron
755 in *C. elegans*. *Dev Cell* **51**, 617-631 e613 (2019).
756 30. S. J. Husson *et al.*, Optogenetic analysis of a nociceptor neuron and network reveals ion
757 channels acting downstream of primary sensors. *Curr Biol* **22**, 743-752 (2012).
758 31. Y. Chen, S. Bharill, E. Y. Isacoff, M. Chalfie, Subunit composition of a DEG/ENaC
759 mechanosensory channel of *Caenorhabditis elegans*. *Proc Natl Acad Sci U S A* **112**,
760 11690-11695 (2015).
761 32. L. Bianchi, M. Driscoll, Protons at the gate: DEG/ENaC ion channels help us feel and
762 remember. *Neuron* **34**, 337-340 (2002).
763 33. M. J. Welsh, M. P. Price, J. Xie, Biochemical basis of touch perception: mechanosensory
764 function of degenerin/epithelial Na+ channels. *J Biol Chem* **277**, 2369-2372 (2002).

765 34. P. G. Gillespie, R. G. Walker, Molecular basis of mechanosensory transduction. *Nature*
766 **413**, 194-202 (2001).
767 35. J. P. Baldin, D. Barth, M. Fronius, Epithelial Na(+) Channel (ENaC) Formed by One or
768 Two Subunits Forms Functional Channels That Respond to Shear Force. *Front Physiol*
769 **11**, 141 (2020).
770 36. A. S. Hill, Y. Ben-Shahar, The synaptic action of Degenerin/Epithelial sodium channels.
771 *Channels (Austin)* **12**, 262-275 (2018).
772 37. D. Mango, R. Nistico, Role of ASIC1a in Normal and Pathological Synaptic Plasticity.
773 *Rev Physiol Biochem Pharmacol* **177**, 83-100 (2020).
774 38. M. N. Gobetto, C. Gonzalez-Inchauspe, O. D. Uchitel, Histamine and Corticosterone
775 Modulate Acid Sensing Ion Channels (ASICs) Dependent Long-term Potentiation at the
776 Mouse Anterior Cingulate Cortex. *Neuroscience* **460**, 145-160 (2021).
777 39. N. W. Bailey, A. J. Moore, Evolutionary Consequences of Social Isolation. *Trends Ecol*
778 *Evol* **33**, 595-607 (2018).
779 40. L. Wilbrecht, A. Holtmaat, N. Wright, K. Fox, K. Svoboda, Structural plasticity underlies
780 experience-dependent functional plasticity of cortical circuits. *J Neurosci* **30**, 4927-4932
781 (2010).
782 41. S. J. Kuhlman, D. H. O'Connor, K. Fox, K. Svoboda, Structural plasticity within the barrel
783 cortex during initial phases of whisker-dependent learning. *J Neurosci* **34**, 6078-6083
784 (2014).
785 42. X. Yu, Y. Zuo, Spine plasticity in the motor cortex. *Curr Opin Neurobiol* **21**, 169-174
786 (2011).
787 43. H. F. Harlow, R. O. Dodsworth, M. K. Harlow, Total social isolation in monkeys. *Proc*
788 *Natl Acad Sci U S A* **54**, 90-97 (1965).
789 44. W. Li, L. Kang, B. J. Piggott, Z. Feng, X. Z. Xu, The neural circuits and sensory channels
790 mediating harsh touch sensation in *Caenorhabditis elegans*. *Nat Commun* **2**, 315 (2011).
791 45. M. Chalfie, J. Sulston, Developmental genetics of the mechanosensory neurons of
792 *Caenorhabditis elegans*. *Dev Biol* **82**, 358-370 (1981).
793 46. J. K. Rose, S. Sangha, S. Rai, K. R. Norman, C. H. Rankin, Decreased sensory
794 stimulation reduces behavioral responding, retards development, and alters neuronal
795 connectivity in *Caenorhabditis elegans*. *J Neurosci* **25**, 7159-7168 (2005).
796 47. J. C. Way, M. Chalfie, *mec-3*, a homeobox-containing gene that specifies differentiation
797 of the touch receptor neurons in *C. elegans*. *Cell* **54**, 5-16 (1988).
798 48. E. M. Hedgecock, J. E. Sulston, J. N. Thomson, Mutations affecting programmed cell
799 deaths in the nematode *Caenorhabditis elegans*. *Science* **220**, 1277-1279 (1983).
800 49. M. Driscoll, M. Chalfie, The *mec-4* gene is a member of a family of *Caenorhabditis*
801 *elegans* genes that can mutate to induce neuronal degeneration. *Nature* **349**, 588-593
802 (1991).
803 50. M. Caneo, V. Julian, A. B. Byrne, M. J. Alkema, A. Calixto, Diapause induces functional
804 axonal regeneration after necrotic insult in *C. elegans*. *PLoS Genet* **15**, e1007863
805 (2019).
806 51. H. Suzuki *et al.*, In vivo imaging of *C. elegans* mechanosensory neurons demonstrates a
807 specific role for the MEC-4 channel in the process of gentle touch sensation. *Neuron* **39**,
808 1005-1017 (2003).
809 52. S. Shi, C. J. Luke, M. T. Miedel, G. A. Silverman, T. R. Kleyman, Activation of the
810 *Caenorhabditis elegans* Degenerin Channel by Shear Stress Requires the MEC-10
811 Subunit. *J Biol Chem* **291**, 14012-14022 (2016).

53. E. R. Sawin, R. Ranganathan, H. R. Horvitz, *C. elegans* locomotory rate is modulated by the environment through a dopaminergic pathway and by experience through a serotonergic pathway. *Neuron* **26**, 619-631 (2000).
54. J. Collet, C. A. Spike, E. A. Lundquist, J. E. Shaw, R. K. Herman, Analysis of osm-6, a gene that affects sensory cilium structure and sensory neuron function in *Caenorhabditis elegans*. *Genetics* **148**, 187-200 (1998).
55. M. Huang, M. Chalfie, Gene interactions affecting mechanosensory transduction in *Caenorhabditis elegans*. *Nature* **367**, 467-470 (1994).
56. Y. Ben-Shahar, Sensory functions for degenerin/epithelial sodium channels (DEG/ENaC). *Adv Genet* **76**, 1-26 (2011).
57. S. Shi, S. M. Mutchler, B. M. Blobner, O. B. Kashlan, T. R. Kleyman, Pore-lining residues of MEC-4 and MEC-10 channel subunits tune the *Caenorhabditis elegans* degenerin channel's response to shear stress. *J Biol Chem* **293**, 10757-10766 (2018).
58. E. L. Tsalik *et al.*, LIM homeobox gene-dependent expression of biogenic amine receptors in restricted regions of the *C. elegans* nervous system. *Dev Biol* **263**, 81-102 (2003).
59. V. A. Alvarez, B. L. Sabatini, Anatomical and physiological plasticity of dendritic spines. *Annu Rev Neurosci* **30**, 79-97 (2007).
60. T. J. Maures *et al.*, Males shorten the life span of *C. elegans* hermaphrodites via secreted compounds. *Science* **343**, 541-544 (2014).
61. T. W. Miller-Fleming *et al.*, The DEG/ENaC cation channel protein UNC-8 drives activity-dependent synapse removal in remodeling GABAergic neurons. *Elife* **5** (2016).
62. J. Aceves, D. Erlij, R. Martinez-Maranon, The mechanism of the paralysing action of tetramisole on Ascaris somatic muscle. *Br J Pharmacol* **38**, 602-607 (1970).
63. E. M. Katz *et al.*, The Stability and Efficacy of Tricaine Methanesulfonate (MS222) Solution After Long-Term Storage. *J Am Assoc Lab Anim Sci* **59(4)**, 393-400 (2020).
64. D. H. Hall, M. Treinin, How does morphology relate to function in sensory arbors? *Trends Neurosci* **34**, 443-451 (2011).
65. M. Hausser, B. Mel, Dendrites: bug or feature? *Curr Opin Neurobiol* **13**, 372-383 (2003).
66. C. Aguirre-Chen, H. E. Bulow, Z. Kaprielian, *C. elegans bicd-1*, homolog of the Drosophila dynein accessory factor Bicaudal D, regulates the branching of PVD sensory neuron dendrites. *Development* **138**, 507-518 (2011).
67. L. DeVault *et al.*, Dendrite regeneration of adult Drosophila sensory neurons diminishes with aging and is inhibited by epidermal-derived matrix metalloproteinase 2. *Genes Dev* **32**, 402-414 (2018).
68. B. A. Gyorffy *et al.*, Local apoptotic-like mechanisms underlie complement-mediated synaptic pruning. *Proc Natl Acad Sci U S A* **115**, 6303-6308 (2018).
69. A. Holtmaat, K. Svoboda, Experience-dependent structural synaptic plasticity in the mammalian brain. *Nat Rev Neurosci* **10**, 647-658 (2009).
70. T. Xu *et al.*, Rapid formation and selective stabilization of synapses for enduring motor memories. *Nature* **462**, 915-919 (2009).
71. G. Yang, F. Pan, W. B. Gan, Stably maintained dendritic spines are associated with lifelong memories. *Nature* **462**, 920-924 (2009).
72. E. N. Star, D. J. Kwiatkowski, V. N. Murthy, Rapid turnover of actin in dendritic spines and its regulation by activity. *Nat Neurosci* **5**, 239-246 (2002).
73. U. V. Nagerl, N. Eberhorn, S. B. Cambridge, T. Bonhoeffer, Bidirectional activity-dependent morphological plasticity in hippocampal neurons. *Neuron* **44**, 759-767 (2004).

859 74. Y. Zhang, R. H. Cudmore, D. T. Lin, D. J. Linden, R. L. Huganir, Visualization of NMDA
860 receptor-dependent AMPA receptor synaptic plasticity in vivo. *Nat Neurosci* **18**, 402-407
861 (2015).
862 75. I. S. Stein, D. K. Park, N. Claiborne, K. Zito, Non-ionotropic NMDA receptor signaling
863 gates bidirectional structural plasticity of dendritic spines. *Cell Rep* **34**, 108664 (2021).
864 76. S. Kellenberger, L. Schild, Epithelial sodium channel/degenerin family of ion channels: a
865 variety of functions for a shared structure. *Physiol Rev* **82**, 735-767 (2002).
866 77. S. Halpain, Avoiding Sibling Conflict: Lessons from Dendrite Self-Avoidance in *C.*
867 *elegans*. *Neuron* **98**, 864 (2018).
868 78. L. Luo, Actin cytoskeleton regulation in neuronal morphogenesis and structural plasticity.
869 *Annu Rev Cell Dev Biol* **18**, 601-635 (2002).
870 79. M. A. Younger, M. Muller, A. Tong, E. C. Pym, G. W. Davis, A presynaptic ENaC
871 channel drives homeostatic plasticity. *Neuron* **79**, 1183-1196 (2013).
872 80. S. Brenner, The genetics of *Caenorhabditis elegans*. *Genetics* **77**, 71-94 (1974).
873 81. E. Kim, L. Sun, C. V. Gabel, C. Fang-Yen, Long-term imaging of *Caenorhabditis elegans*
874 using nanoparticle-mediated immobilization. *PLoS One* **8**, e53419 (2013).
875

Figures

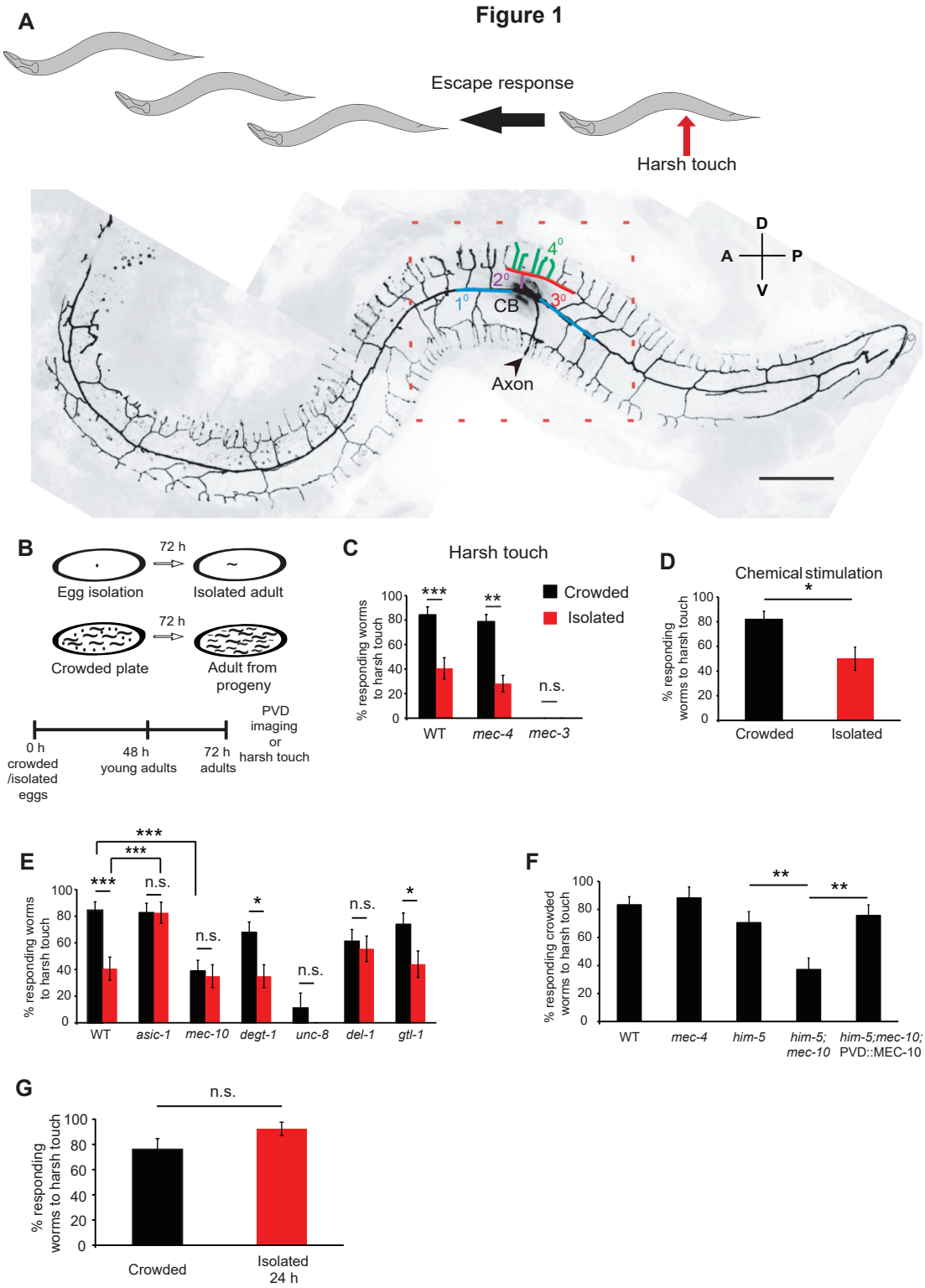
Figure 1
A
Escape response
Harsh touch
D
A
P
V
4°
2°
1°
3°
CB
Axon
B
72 h
Egg isolation
Isolated adult
72 h
Crowded plate
Adult from progeny
0 h crowded /isolated eggs
48 h young adults
72 h adults
PVD imaging or harsh touch
C
Harsh touch
Crowded
Isolated
% responding worms to harsh touch
***
**
n.s.
WT
mec-4
mec-3
D
Chemical stimulation
*
% responding worms to harsh touch
Crowded
Isolated
E
% responding worms to harsh touch
***
***
***
n.s.
n.s.
*
n.s.
n.s.
*
WT
asic-1
mec-10
degt-1
unc-8
del-1
gtl-1
F
% responding crowded worms to harsh touch
**
**
WT
mec-4
him-5
him-5; mec-10
him-5;mec-10; PVD::MEC-10
G
n.s.
% responding worms to harsh touch
Crowded
Isolated 24 h

878 **Figure 1. Mechanosensory deprivation during development reduces the**
879 **behavioral response of the PVD neuron. (A)** The PVD neuron dendritic tree, cell body
880 (CB) and axon. The red arrow corresponds to the contact point with a platinum wire
881 during posterior harsh touch, while the black arrow represents the behavioral escape
882 response of the worm. The red dashed square represents the analyzed region around
883 the CB. One representative candelabrum is colored by branch orders: blue primary (1°),
884 purple secondary (2°), red tertiary (3°) and green quaternaries (4°). A- anterior; P-
885 posterior; V- ventral; D-dorsal. **(B)** Schematic of the isolation protocol followed at 72 h
886 by posterior harsh touch assay or PVD imaging of adult worms. **(C)** Isolation of embryos
887 reduced the percentage of worms responding to harsh touch at adulthood. Crowded-
888 black bars, Isolated- red bars. Wildtype (WT) N2 worms (Crowded, n=32; Isolated,
889 n=32), *mec-4* (Crowded, n=52; Isolated, n=46), *mec-3* (Crowded, n=12; Isolated, n=12).
890 *mec-4* animals were assayed as adults after 96 h to account for their slower rate of
891 growth. **(D)** Growth in plates with chemical cues from adult hermaphrodites did not alter
892 the reduced response rate of isolated *mec-4* animals to harsh touch (Crowded, n=33;
893 Isolated, n=28). **(E)** Harsh touch response in crowded and isolated conditions for
894 mutants of different DEG-ENaCs and the TRP channel *gtl-1*. WT worms (same set of
895 worms as in Fig. 1C. Crowded, n=32; Isolated, n=32), *asic-1* (Crowded, n=46; Isolated,
896 n=30), *mec-10* (Crowded, n=38; Isolated, n=31), *degt-1* (Crowded, n=37; Isolated,
897 n=31), *unc-8* (Crowded, n=18; Isolated, n=15), *del-1* (Crowded, n=31; Isolated, n=27),
898 *gtl-1* (Crowded, n=27; Isolated, n=25). **(F)** MEC-10 expression in the PVD rescues *mec-*
899 *10* mutants' crowded-specific reduction in response to harsh touch. All strains contain
900 the *ser-2Prom3::Kaede* PVD marker construct, and were tested in the crowded
901 conditions. (WT, n=42; *mec-4,* n=17; *him-5,* n=34 (*him-5* was used as WT background
902 for several strains after cross); *him-5;mec-10,* n=35; *him-5;mec-10*;*ser2Prom3*::MEC-
903 10, n=33). **(G)** Isolation for 24 h in adulthood did not affect the response to harsh touch.
904 Worms grown under crowded conditions were isolated for 24 h as young adults and
905 compared against their crowded age-matched counterparts in their response to harsh
906 touch (Crowded, n=25; Isolated for 24 h, n=26). The proportion of responding worms
907 (percentage) ± standard error of proportion is shown. Fisher's exact test, *$p<0.05$,
908 **$p<0.01$, ***$p<0.001$, n.s. not significant.
909

Figure 2

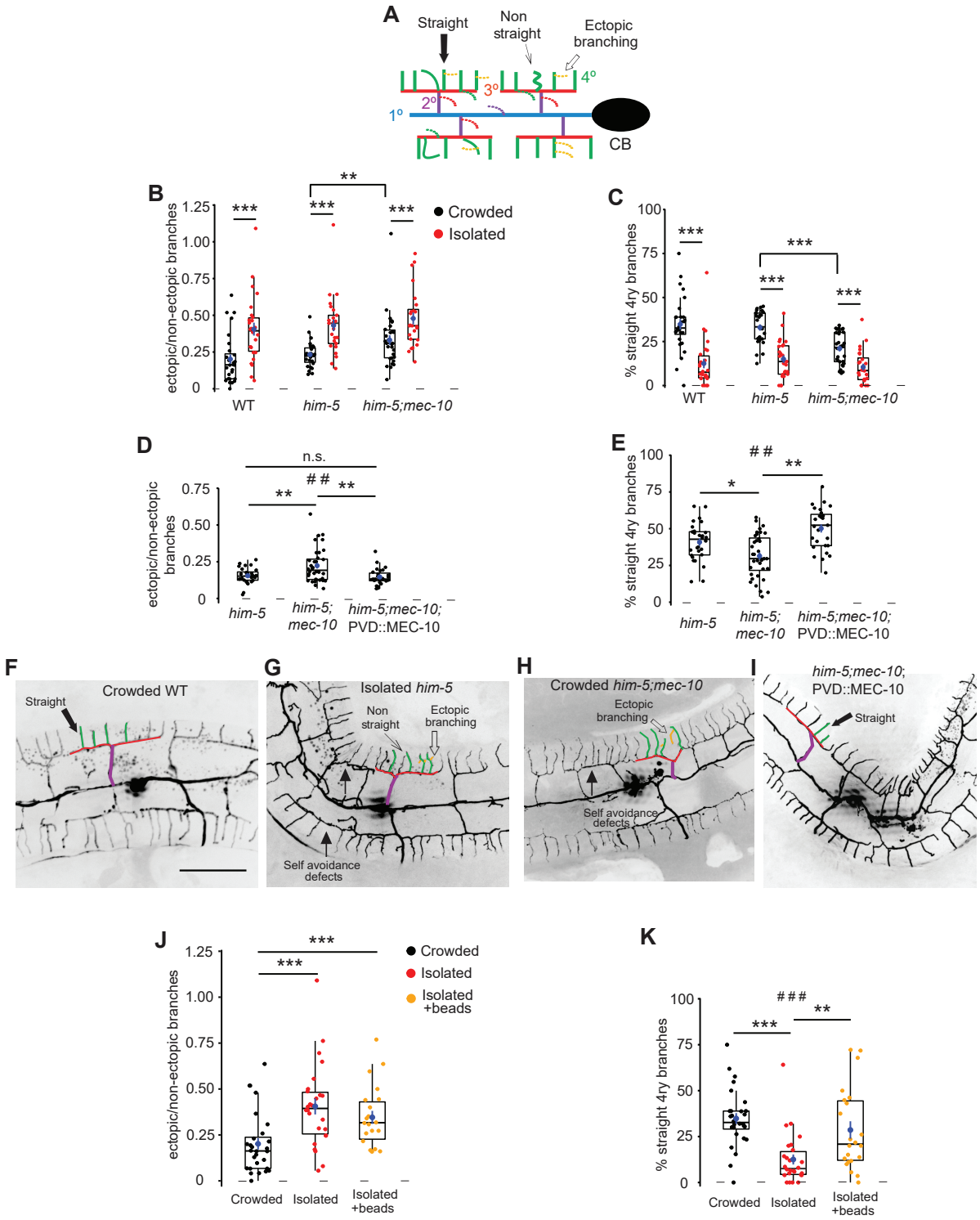
A
Straight
Non straight
Ectopic branching
1°
2°
3°
4°
CB
B
ectopic/non-ectopic branches
Crowded
Isolated
WT
him-5
him-5;mec-10
C
% straight 4ry branches
D
ectopic/non-ectopic branches
n.s.
him-5
him-5; mec-10
him-5;mec-10; PVD::MEC-10
E
% straight 4ry branches
F
Crowded WT
Straight
G
Isolated him-5
Non straight
Ectopic branching
Self avoidance defects
H
Crowded him-5;mec-10
Ectopic branching
Self avoidance defects
I
him-5;mec-10; PVD::MEC-10
Straight
J
ectopic/non-ectopic branches
Crowded
Isolated
Isolated +beads
K
% straight 4ry branches

Figure 2. Mechanosensory deprivation and cell autonomous activity of *mec-10* affects the architecture of the PVD. (A) Schematic representation of the PVD dendritic structure, marking the morphological characteristics of interest: ectopic branches and quaternary branching geometry. Dashed lines represent ectopic branching at each order. Colors correspond to Fig. 1A. (**B-G**) Both isolation and *mec-10* affect the structure of the PVD: **(B)** Isolation increases the fraction of ectopic branching, *mec-10* mutation increases ectopic branching in the crowded state. **(C)** Isolation decreases the percentage of straight quaternary branches, *mec-10* mutation decreases the percentage of straight quaternary branches in the crowded state. Crowded- black dots, isolated- red dots; WT (Crowded, n=28; Isolated n=26), *him-5* (Crowded, n=27; Isolated, n=25; *him-5* was used as WT background for several strains after cross), *him-5;mec-10* (Crowded, n=30; Isolated, n=24). **(D)** Expression of *mec-10* in the PVD on the background of *him-5;mec-10* in the crowded state reduces ectopic branching and **(E)** increases the percentage of straight quaternary branches. **(F-I)** Representative PVD images of WT, *mec-10* and *mec-10*;PVD::MEC-10 in different growth conditions. (Scale bar, 50 μm). **(J)** Embryo isolation with glass beads did not affect ectopic branching. **(K)** Embryo isolation with glass beads increased the percentage of straight quaternary branches (Crowded, n=28; Isolated n=26; Isolated with beads, n=22. Crowded and isolated WT are the same set of worms as in Fig. 2B,C). Each dot represents a single worm. The mean ± s.e.m. are shown in blue. Box plot with median and hinges for the first and third quartile. The whiskers represent an estimated calculation of the 95% confidence interval. Kruskal-Wallis test, # # $p<0.01$, # # # $p<0.001$, Mann Whitney test with Bonferroni Correction $\alpha=0.0167$. *$p<0.05$, ** $p<0.01$, *** $p<0.001$, n.s. not significant.

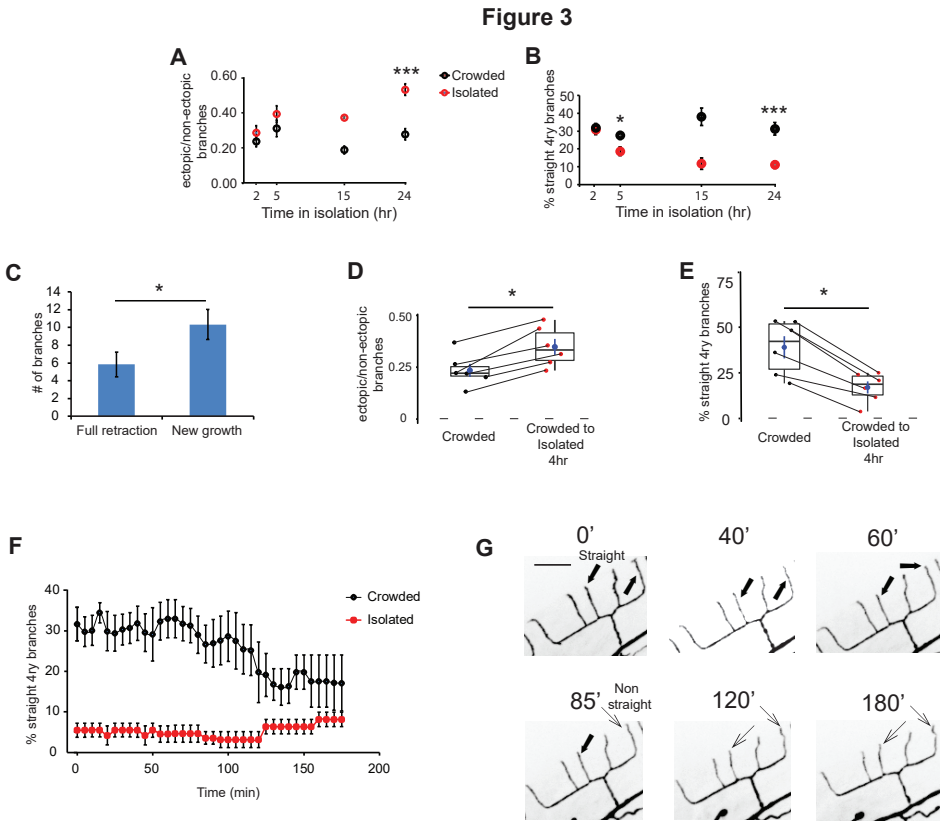

Figure 3. Adult isolation for less than 4 h affects the structure of the PVD. **(A)** Isolation of crowded worms induces a time-dependent increase in the proportion of ectopic branches, and **(B)** a decrease in the number of straight quaternary branches (2 h: Crowded, n=24, Isolated, n=22; 5 h: Crowded, n=24, Isolated, n=27; 15 h: Crowded, n=3, Isolated, n=3; 24 h: Crowded, n=20, Isolated, n=21; animals imaged using polystyrene beads for immobilization, see Materials and Methods). **(C)** Isolation for 4 h induces more growth of new branches than retraction of existing ones. Ectopic branch dynamics were compared for crowded animals against their state after 4 h isolation. Imaging used 1% tricaine, see Materials and Methods. **(D)** Isolation of crowded worms for 4 h increases the ratio between ectopic/non-ectopic branches in individual animals and **(E)** reduces the percentage of straight quaternary branches (Crowded, n=6; Isolated n=6). **(F)** Crowded, but not isolated worms, show dynamic reduction in the percentage of straight quaternary branches during a 3 h time lapse movie in 1% tricaine; see Movies S5 and S6. **(G)** Representative time lapse frames of a crowded worm in 1% tricaine. Thick and thin arrows represent straight and non-straight quaternary branches, respectively. For **(D, E)** the lines connecting two points refer to the same crowded specimen at time 0 and after 4 h isolation. Box plot representation as in Fig. 2. For **(A-B)** Mann-Whitney test, * $p<0.05$,.*** $p<0.001$. For **(C-E)** Wilcoxon test (for two related samples), * $p<0.05$.

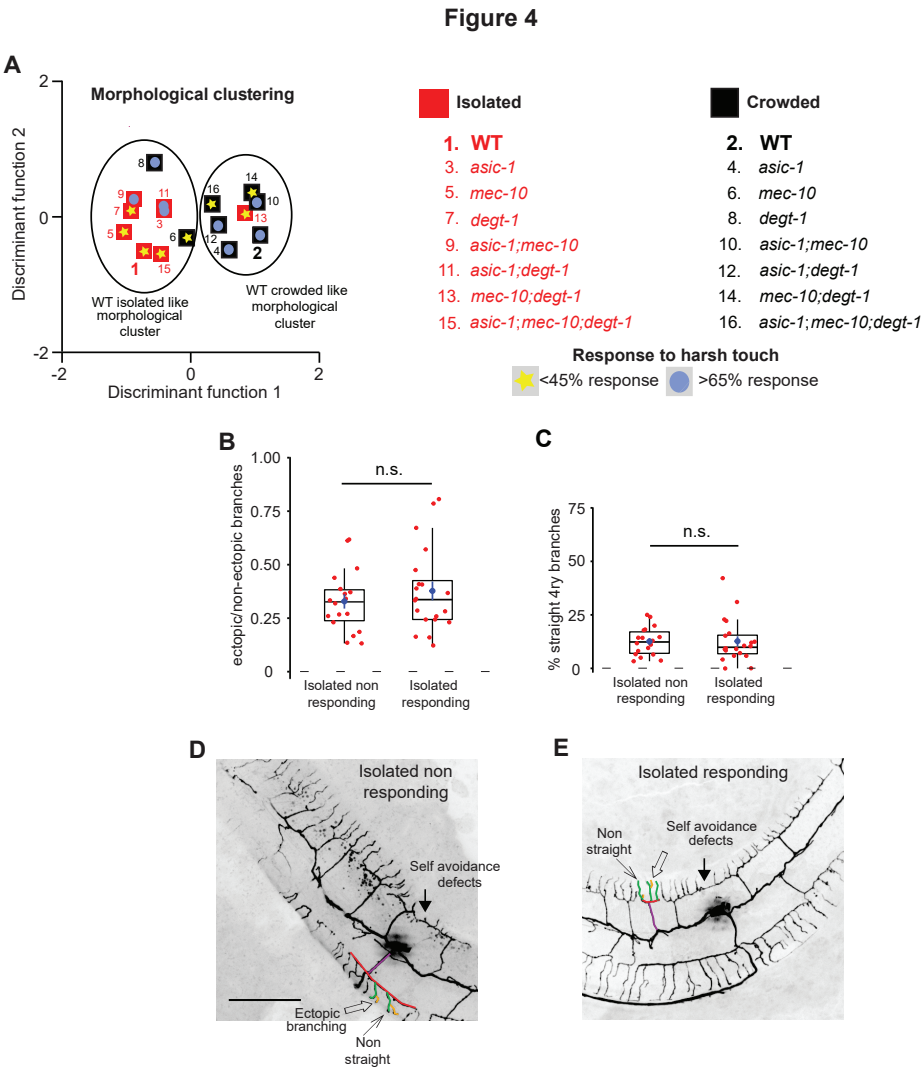

Figure 4. Response to harsh touch and PVD morphology are independent. **(A)** Discriminant analysis shows independence of harsh touch response from the PVD's morphological classification. Squares indicate the centroids for morphological characteristics analyzed in Fig. S10A-C. The response to harsh touch (Fig. S9) is illustrated by its magnitude (low, <45% in yellow star; high, >65% in light blue circles). The different genotypes are numbered in the list on the right. Crowded- black, Isolated- red. **(B-E)** Isolated animals show similar PVD morphology regardless of their touch response: **(B)** isolated responding and non-responding animals are not different with regard to the fraction of ectopic branching, and **(C)** the geometry of quaternary branches (Isolated non-responding, n=18; Isolated responding, n=20). Box plot representation as in Fig. 2. Mann-Whitney test. n.s. not significant. **(D, E)** Representative PVD images of responding and non-responding worms. (Scale bar, 50 µm).

Figure 5

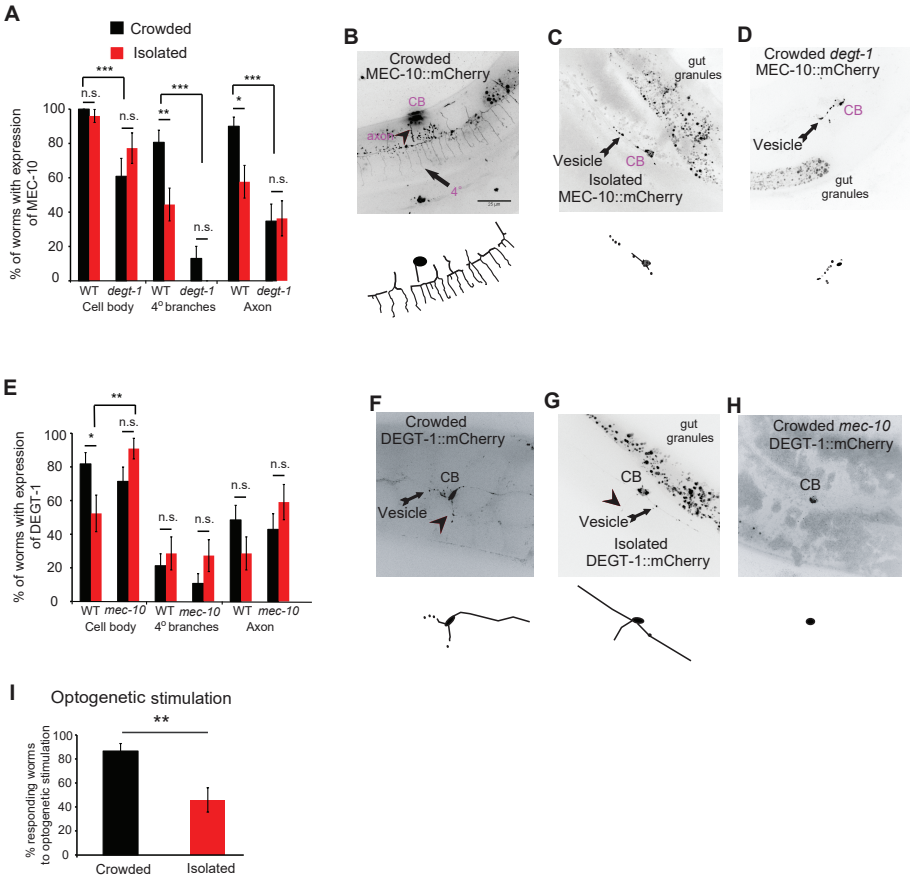

Figure 5. Mechanosensory-dependent localization of degenerins and optogenetics. (A) PVD::MEC-10::mCherry localization (shown and labeled in purple, also in Fig. 7) is reduced in the quaternary branches and the axon following isolation, in a *degt-1*-dependent manner (WT: Crowded, n=31; Isolated, n=27; *degt-1* mutants: Crowded, n=23; Isolated, n=22). **(B-D)** Representative images and reconstructions for PVD::MEC-10::mCherry localization for crowded and isolated WT worms, and crowded *degt-1* worms. (Scale bar, 50 µm). **(E)** PVD::DEGT-1::mCherry localization level is reduced at the cell body, but not in the quaternary branches or the axon, following isolation, in a *mec*-10-dependent-manner (WT: Crowded, n=33; Isolated, n=21; *mec-10* mutants: Crowded, n=28; Isolated, n=22). The percentage of expressing worms ± standard error of proportion is shown. **(F-H)** Representative images and reconstructions for PVD::DEGT-1::mCherry localization for crowded and isolated WT worms and crowded *mec-10* worms. **(I)** Isolation leads to a reduced escape response following optogenetic photoactivation of Channelrhodopsin 2 in the PVD (Crowded, n=30; Isolated, n=24, grown on All Trans Retinal. No response was observed for worms grown without All Trans Retinal). Fisher exact test, *p<0.05, **p<0.01, ***p<0.01 n.s. not significant.

Figure 6

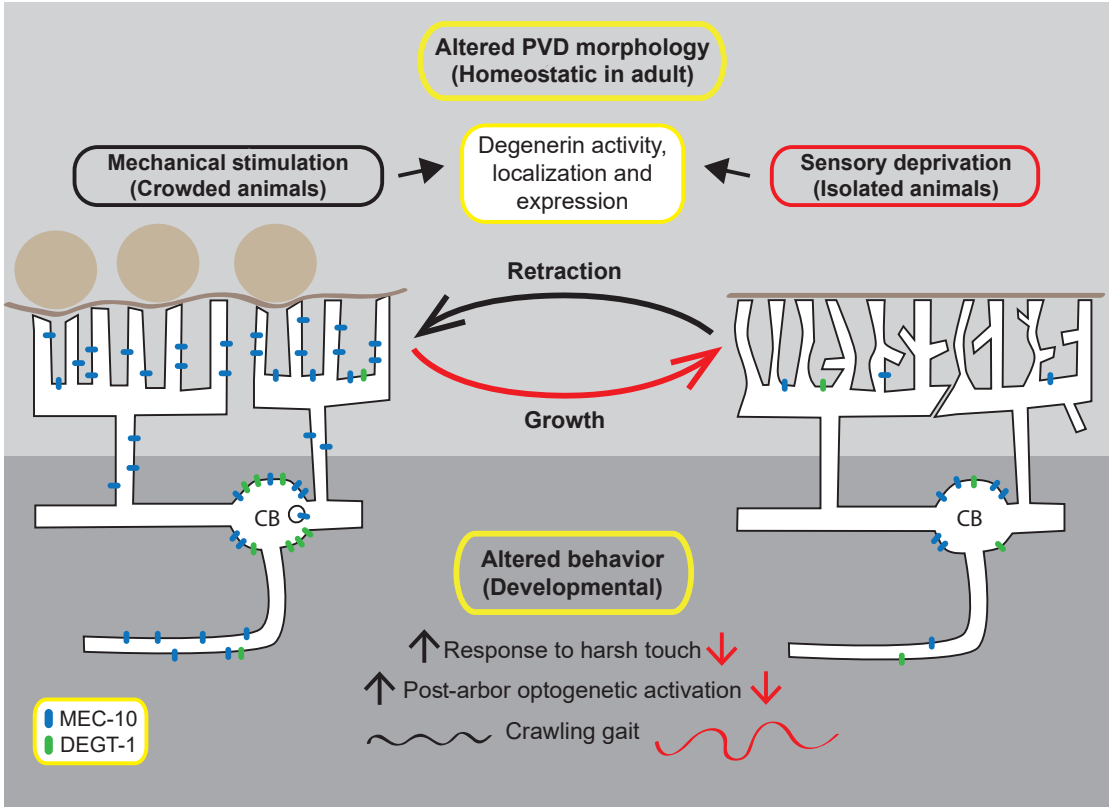

Figure 6. Model of experience-induced structural and behavioral plasticity. During adulthood, mechanosensory signals maintain the structure of the PVD in crowded animals, with straight quaternary branches and fewer ectopic branches. Sensory deprivation (in isolated animals) results in ectopic dendrites, wavy branches and defects in candelabra self-avoidance. During development, mechanosensory experience alters the response to harsh touch and the crawling gait of the worm, possibly through changes in MEC-10 localization in the axon and mediated by other DEG/ENaCs. Mechanosensory stimuli are a driving force for changes in the compartment specific localization of MEC-10 and DEGT-1 in the PVD, which may affect the structure of the PVD. MEC-10 is represented in blue, DEGT-1 is represented in green.